## Dalton Transactions



Cite this: Dalton Trans., 2011, 40, 3808

www.rsc.org/dalton PAPER

# Dye-sensitized solar cells based on TiO<sub>2</sub>-B nanobelt/TiO<sub>2</sub> nanoparticle sandwich-type photoelectrodes with controllable nanobelt length

Youzhen Dong,<sup>a</sup> Kai Pan,<sup>a</sup> Guohui Tian,<sup>a</sup> Wei Zhou,<sup>a</sup> Qingjiang Pan,<sup>a</sup> Tengfeng Xie,<sup>b</sup> Dejun Wang<sup>b</sup> and Honggang Fu\*<sup>a</sup>

Received 20th December 2010, Accepted 21st January 2011 DOI: 10.1039/c0dt01799j

The  $TiO_2$ -B nanobelt (NB)/ $TiO_2$  nanoparticle (NP) sandwich-type structure photoelectrode, with controllable nanobelt length, has been used to fabricate high-efficiency dye-sensitized solar cells (DSSCs), which combine the advantages of the rapid electron transport in  $TiO_2$ -B NBs and the high surface area of  $TiO_2$  NPs. The results indicate that the sandwich-type photoelectrode achieves higher photoelectrical conversion efficiency when compared with the  $TiO_2$  nanoparticulate electrode. Increasing the length of  $TiO_2$ -B NBs has been demonstrated to improve the photoelectric conversion efficiency ( $\eta$ ). DSSCs with the longest ( $10~\mu m$ )  $TiO_2$ -B NBs yield the highest  $\eta$  of 7.94%. The interfacial electron transport of DSSCs with different lengths of  $TiO_2$ -B NBs has been quantitatively investigated using the photovoltage transient and the electrochemical impedance spectra, which demonstrates that the DSSCs with longest  $TiO_2$ -B NBs display the highest electron collection efficiency and the fastest interfacial electron transfer.

## 1. Introduction

Since the outstanding work of M. Grätzel in 1991, dye-sensitized solar cells (DSSCs) have become a possible economical alternative to the conventional solar energy cells.<sup>1-4</sup> Generally, DSSCs are composed of nanocrystalline semiconductor oxide photoelectrode, dye sensitizers, redox shuttle and counter electrode. 5,6 Under illumination, an electron is injected into the conduction band of the semiconductor photoelectrode from the excited state of the sensitizer. The oxidized dye can be recovered by a suitable redox shuttle. The diffusion of the oxidized shuttle to the counter electrode completes the circuit.<sup>7-9</sup> Along with these processes, the photo-generated electron transport and recombination are the key factors to determine the performance of DSSCs. In principle, a fast photoelectron transfer and slow recombination will result in a higher photoelectrical conversion efficiency  $(\eta)$ . The photoelectron transfer and recombination mainly depend on the structure of the photoelectrodes, therefore, optimizing the structure of the photoelectrode is necessary for developing highlyefficient DSSCs.10

An anatase TiO<sub>2</sub> nanoparticle (NP) film is an excellent starting photoelectrode for DSSCs due to its facile fabrication and low cost. <sup>11-13</sup> However, the small electron diffusion coefficient limits

the random walk of electrons through the NP film. A Recently, some strategies have been attempted to optimize the structure of the photoelectrodes to increase the  $\eta$  of DSSCs. One strategy was to replace the TiO<sub>2</sub> NP with bead-like TiO<sub>2</sub>, mesoporous TiO<sub>2</sub> and so on. The other promising strategy was to apply one-dimensional (1D) nanomaterials including nanowires (NWs), nanotubes (NTs) and nanorods because these materials can accelerate electron transport and increase light scattering. Electron transport in 1D nanomaterials is expected to be several orders of magnitude faster than percolation through a random nanoparticle network. Unfortunately, these 1D nanomaterials suffer from a much lower surface area, with roughness factors (RF) < 200, than nanoparticulate films (RF > 1000), which reduces the photocurrent density significantly and thus results in a lower  $\eta$  of the DSSCs.

Since the NPs can provide a high surface area to facilitate the dye adsorption and the 1D nanomaterials can enhance the photo-generated electron transport and light scattering, a 1D nanomaterial/NP composite could be an ideal structure for the fabrication of DSSC photoelectrodes. So far, there have been several investigations on this system, including TiO<sub>2</sub> NW/NP and ZnO NW/TiO<sub>2</sub> NP composite solar cells. <sup>24,25</sup> The studies showed that the  $\eta$  was improved through the combination of NWs and NPs and the 1D TiO<sub>2</sub> nanostructure yielded better results than the 1D ZnO one. <sup>26</sup> However, the TiO<sub>2</sub> NWs composed of anatase phase can only be obtained through a complicated preparation procedure or high temperature annealing. Therefore, synthesizing a 1D nanostructure *via* simple methods and clarifying the mechanism for the enhanced  $\eta$  is still a promising work.

<sup>&</sup>quot;Key Laboratory of Functional Inorganic Material Chemistry (Heilongjiang University), Ministry of Education, School of Chemistry and Materials Science, Heilongjiang University, Harbin 150080, People's Republic of China. E-mail: fuhg@vip.sina.com; Fax: +86 451 8667 3647; Tel: +86 451 8660 8458

<sup>&</sup>lt;sup>b</sup>College of Chemistry, Jilin University, Changchun 130012, People's Republic of China

Due to their edge and corner sharing TiO<sub>6</sub> octahedra and relatively open structure, TiO<sub>2</sub>-B NTs and NWs have attracted much attention.<sup>27,28</sup> TiO<sub>2</sub>-B NTs and NWs exhibit high lithium intercalation capacity, high discharge/charge rate capability, excellent photocatalytic activity and a good electrochemical performance and they can be easily prepared by hydrothermal method. So, 1D TiO<sub>2</sub>-B nanomaterials/TiO<sub>2</sub> NP composite may be a good candidate for DSSC photoelectrode materials.

In this work, TiO<sub>2</sub>-B nanobelts (NBs) with different lengths have been obtained by the hydrothermal or solvothermal methods. The TiO<sub>2</sub>-B NB/TiO<sub>2</sub> NP sandwich-type structure photo-electrodes with different NB lengths have been used to fabricate DSSCs, which possess the merits of their building blocks, i.e. the rapid electron transport rate of TiO2-B NBs and the high surface area of TiO<sub>2</sub> NPs. The DSSCs with such a sandwich structure photoelectrode achieved enhanced photoelectrical conversion efficiency. It was found that the cells with the longest (10 µm) TiO<sub>2</sub>-B NBs yielded the highest  $\eta$  of 7.94%. The interfacial electron transport of DSSCs with different lengths of TiO2-B NBs was systematically investigated by the photovoltage transient and the electrochemical impedance spectra (EIS), which demonstrated that the longest TiO2-B NB/TiO2 NP sandwich-type DSSCs exhibited the best electron collection efficiency and the fastest interfacial electron transfer.

## 2. Results and discussion

### 2.1. Structure characterization of TiO<sub>2</sub>-B NBs

Fig. 1 shows the typical XRD patterns of  $\text{TiO}_2\text{-B}$  NBs with different lengths. The long (10 µm)  $\text{TiO}_2\text{-B}$  NBs are labelled as L-TiO<sub>2</sub>-B NBs and the middle (4 µm) and short (500 nm)  $\text{TiO}_2\text{-B}$  NBs are labelled as M-TiO<sub>2</sub>-B NBs and S-TiO<sub>2</sub>-B NBs, respectively. All the samples exhibit characteristic peaks around  $2\theta = 14.18^\circ$ ,  $25.10^\circ$ ,  $29.70^\circ$ ,  $44.34^\circ$  and  $48.54^\circ$ , which correspond to the (001), (110), ( $\overline{4}$ 03), ( $\overline{6}$ 01) and (020) planes of TiO<sub>2</sub>-B (JCPDS 46-1238). Further confirmation of the formation of the TiO<sub>2</sub>-B was obtained from the laser Raman spectra (Fig. 2). The Raman spectra acquired with TiO<sub>2</sub>-B NBs shows the same response peaks and the band positions for the TiO<sub>2</sub>-B phase are in excellent

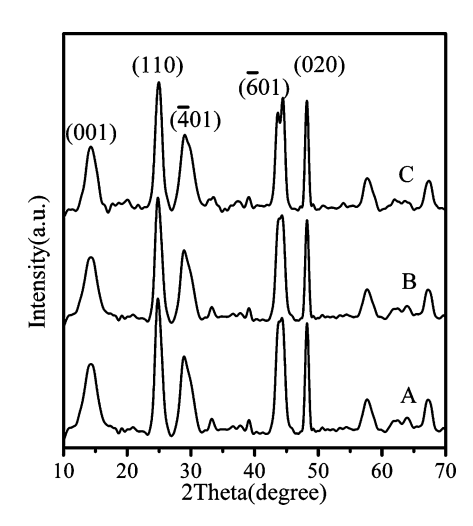


**Fig. 1** XRD patterns of L-TiO<sub>2</sub>-B NBs (a), M-TiO<sub>2</sub>-B NBs (b) and S-TiO<sub>2</sub>-B NBs (c).

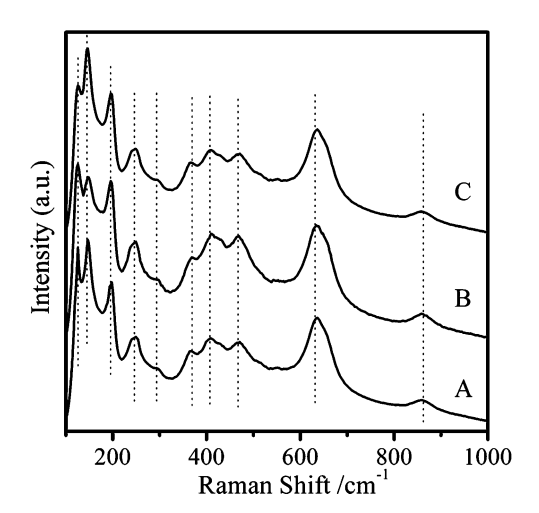


**Fig. 2** Raman spectra of L-TiO<sub>2</sub>-B NBs (a), M-TiO<sub>2</sub>-B NBs (b) and S-TiO<sub>2</sub>-B NBs (c).

agreement with the published data on either bulk or nanowires.<sup>29–31</sup> No anatase or rutile TiO<sub>2</sub> can be detected, which indicates that the starting TiO<sub>2</sub> has been fully converted into TiO<sub>2</sub>-B nanostructures. Evidence that the 1D TiO<sub>2</sub>-B have different lengths is shown in Fig. 3. As shown in Fig. 3 (a, b), the length of L-TiO<sub>2</sub>-B NBs is about 10 μm. The morphology of M-TiO<sub>2</sub>-B NBs is shown in Fig. 3 (c, d) and their length is  $\sim 4 \,\mu m$ . The length of S-TiO<sub>2</sub>-B NBs is about 500 nm, Fig. 3 (e, f). All of the 1-D TiO<sub>2</sub>-B have the same diameter of ca. 100 nm. High-resolution TEM (HRTEM) images (inset in Fig. 3 (b. d. f)) show clearly the well-crystallized layered structure of TiO<sub>2</sub>-B with the interlayer spacing of about 0.37 and 0.65 nm. The lattice parameters were found to be in agreement with those of TiO<sub>2</sub>-B (a = 1.220 nm, b = 0.3748 nm, c = 0.6535 nm and  $\beta =$ 107.36°).<sup>29</sup> Therefore, in conjunction with uniform diameter, TiO<sub>2</sub>-B NBs with long, middle and short lengths (10 μm, 4 μm, 500 nm) have been obtained.

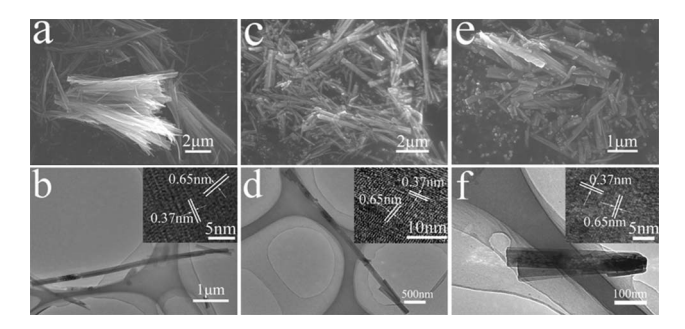


**Fig. 3** SEM and TEM images of L-TiO<sub>2</sub>-B NBs (a, b), M-TiO<sub>2</sub>-B NBs (c, d), and S-TiO<sub>2</sub>-B NBs (e, f). Inset are HRTEM images corresponding to b, d and f.

## 2.2. The surface photovoltage spectra (SPS) of TiO<sub>2</sub>-B NBs

Surface photovoltage is a well-established contactless technique for semiconductor characterization, which relies on analyzing the illumination-induced change of the surface voltage. SPS provides information about the properties of the sample surface layer (several atomic layers), containing the separation capability of the photo-generated electrons and holes, the bandgap of the semiconductor and so on.<sup>32</sup> The SPS of TiO<sub>2</sub>-B NBs with different

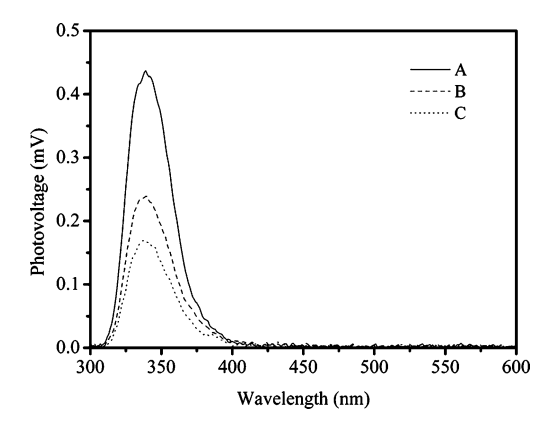


Fig. 4 The SPS of L-TiO<sub>2</sub>-B NBs (a), M-TiO<sub>2</sub>-B NBs (b) and S-TiO<sub>2</sub>-B NBs (c).

lengths have been shown in Fig. 4. It can be clearly seen that there was a photovoltage response peak at the wavelength of 338 nm, which was attributed to band-band transition of the TiO<sub>2</sub>-B NBs. So, the investigation indicates that TiO<sub>2</sub>-B NBs are potential photoelectrical materials for application in DSSCs.

## 2.3. Photoelectrical character of DSSCs with sandwich-type photoelectrodes

Because the 1-D TiO<sub>2</sub>-B NBs possess fast photo-electron transportation and the NPs have higher surface area, the sandwichtype photoelectrodes would exhibit the merits of the two building blocks, i.e. the high surface area of TiO2 NPs and the rapid interfacial electron transport of 1-D TiO<sub>2</sub>-B. So, sandwich-type photoelectrodes with 1-D TiO2-B of different lengths have been fabricated in order to obtain a higher  $\eta$  for DSSCs. The sandwichtype photoelectrodes with L-TiO<sub>2</sub>-B NBs are labeled as PLs and the photoelectrodes with M-TiO<sub>2</sub>-B NBs and S-TiO<sub>2</sub>-B NBs are labeled as PMs and PSs, respectively. An electrode with two layers of TiO<sub>2</sub> NP thin films is also prepared (labled as PTs). The fabricated DSSCs are labelled as CLs, CMs, CSs and CTs, respectively. The typical photocurrent photovoltage curves of CLs, CMs, CSs and CTs are shown in Fig. 5. The film photoelectrodes were shared with the same batch. Each value for cell performance was taken as an average of at least 3 samples.

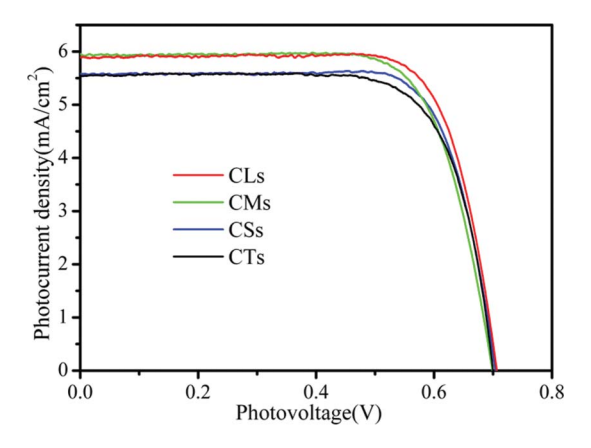


Fig. 5 Photocurrent density-photovoltage curves of CLs, CMs, CSs and CTs.

**Table 1** Solar cell parameters of CLs, CMs, CSs and CTs, respectively<sup>a</sup>

Cells	$V_{oc}(V)$	$I_{\rm sc}$ (mA cm <sup>-2</sup> )	FF	η (%)
CLs	0.71	5.89	0.76	7.94
CMs	0.70	5.95	0.73	7.63
CSs	0.70	5.57	0.76	7.47
CTs	0.70	5.55	0.74	7.20

<sup>a</sup>  $I_{sc}$ : short-circuit photocurrent.  $V_{oc}$ : open-circuit photovoltage. FF: fill factor.  $\eta$ : power conversion efficiency.

The values of the open circuit voltage  $(V_{oc})$ , short-circuit current  $(I_{sc})$ , fill factor (FF) and overall photoelectrical conversion efficiency  $(\eta)$ , obtained from the curves, are summarized in Table 1. The photoelectrical properties of the cells with the TiO<sub>2</sub>-B NB/TiO<sub>2</sub> NP sandwich-type photoanodes are higher than the control cells (CTs). Especially, CLs achieved the highest photoelectrical conversion performance of 7.94%, resulting from a  $V_{\rm oc}$  of 0.71V, a  $I_{\rm sc}$  of 5.89 mA cm<sup>-2</sup> and a FF of 0.76. In comparison with CTs, the  $\eta$  of CLs increases by ca. 10.3%. Accordingly, the CMs have a lower  $\eta$  of 7.63% and the CSs have a much lower  $\eta$  of 7.47%, than that of the CLs. This means that the lengths of the TiO<sub>2</sub>-B NBs play a significant role on the conversion efficiency of the DSSCs using the present sandwichstructure photoelectrode. Increasing the length of the TiO<sub>2</sub>-B NBs can improve the performance of DSSCs effectively. It should be noted that the amount of adsorbed dye molecules will also affect the conversion efficiency of the DSSCs. It is possible that more dye adsorption would result in a higher power photoelectrical conversion efficiency. According to the Beer-Lambert law, the molar concentration of dve loading from CLs, CMs, CSs and CTs is 2.1, 2.2, 1.9 and  $2.4 \times 10^{-7}$  mol cm<sup>-2</sup>, respectively.<sup>33</sup> These photoelectrodes based on TiO<sub>2</sub>-B NBs have approximately the same dye adsorption amount. Therefore, we do not think the improved conversion efficiency by the length of TiO2-B NBs results from a different amount of adsorbed dve molecules. In the following, the photo-electron transfer properties of DSSCs with sandwich-type photoelectrode are systematically studied with EIS and the photovoltage transient.

## 2.4. Interfacial charge transfer studied by EIS

EIS is one of the powerful methods used to investigate internal resistance, which is an indicator of the charge transfer process of DSSCs. The wide frequency range of the EIS enables the measurement of the wide scale internal resistance of each electrochemical step at the same time. The DSSC is a complex system composed of several interfaces. A high electron accumulation must occur because photo-generated electrons are not extracted at the electrode contact under illumination. Electron transport and recombination in the photoelectrode, charge transfer reactions at the Pt counter electrode and the diffusion constant of I<sub>3</sub>- can all be studied by EIS.<sup>34</sup> Usually, the impedance at low frequency (0.05–1 Hz) corresponded to the Nernst diffusion of  $I_3^-/I^-$  within the electrolyte. The impedance at high frequency (1 K–100 K Hz) in the impedance spectra corresponded to the capacitance and charge-transfer resistance at the Pt  $\mid I_3^-/I^-$  electrolyte interface.

The medium-frequency response at 1-1 K Hz was associated with the photoelectrode-dye | I<sub>3</sub>-/I- electrolyte interface, where an accumulation of photoelectrons and redox shuttles are expected.35,36 EIS were obtained by applying sinusoidal perturbations of 10 mV over the  $V_{oc}$ . Fig. 6 shows the Nyquist diagrams of the impedance spectra of CLs, CMs, CSs and CTs under illumination of 10 mW cm<sup>-2</sup>. In general, the Nyquist diagram obtained under a light intensity of 100 mW cm<sup>-2</sup> exhibits three semicircles, which correspond to three frequency ranges. However, in this experiment, only the semicircles at the middle and high frequencies were observed, associated with the dye-sensitized photoelectrode | I<sub>2</sub><sup>-</sup>/I<sup>-</sup> electrolyte interface and the Pt | I<sub>2</sub><sup>-</sup>/I<sup>-</sup> electrolyte interface resistance, respectively. The semicircle at the low frequency region merges with the semicircle at the middle frequency region due to the weak light intensity.<sup>37</sup>

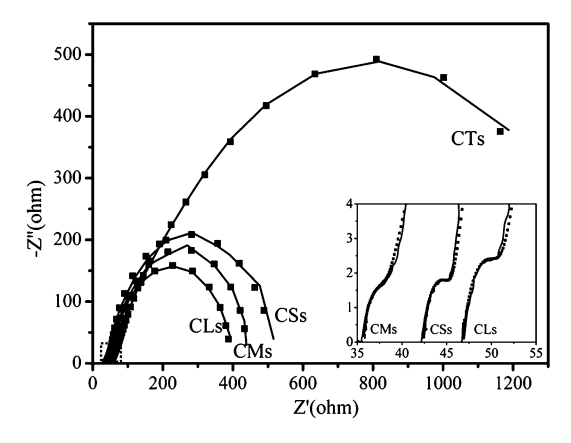


Fig. 6 Nyquist diagrams of the impedance spectra of CLs, CMs, CSs and CTs under illumination of 10 mW cm<sup>-2</sup>. Inset is the magnification of the high-frequency region.

Many theoretical models have been proposed to interpret the complex system of the DSSC under different conditions. The equivalent model fitting of the impedance spectra of CLs, CMs, CSs and CTs is shown in Fig. 7. The symbols of R and C represent a resistance and a capacitance, respectively.  $R_1$  is a series resistance, standing for the transport resistance of the two TCO electrodes. If the thickness of the  $TiO_2$  film is L, the  $R_{ct}$  (=  $r_{ct}/L$ ) represents the charge transfer resistance between the sandwichtype film photoelectrode and  $I_3^-$  in the electrolyte.  $C_1$  (=  $c_1L$ ) is the chemical capacitance of the sandwich-type film photoelectrode, which accounts for the change of electron density as a function of the Fermi level.  $Z_{Dif}$  represents the Warburg impedance relative to the Nernst diffusion of I<sub>3</sub><sup>-</sup> in the electrolyte, where the impedance of the finite-length Warburg diffusion can be expressed by eqn 1.

$$Z_{Dif} = R_{Dif} \left\{ \begin{bmatrix} \tanh(j\omega\tau)^{1/2} \\ /(j\omega\tau)^{1/2} \end{bmatrix} \right\}$$
 (1)

Where  $R_{\rm Dif} = B/Y_{\rm O1}$ ,  $\tau = B^2$ , B was parameter.  $R_2$  and  $C_2$  are the charge-transfer resistance and double-layer capacitance at the counter electrode, respectively.

The EIS data obtained by fitting the impedance spectra of CLs, CMs, CSs and CTs using the equivalent model of Fig. 7 are shown in Table 2. The EIS data in this work are helpful for the understanding of all sandwich-type structure solar cells, and also can explain the existing interfaces in DSSCs. The  $R_{ct}$ value is the key parameter that determines the interfacial electron transfer of DSSCs. It can be clearly seen that  $R_{ct}$ , representing

**Table 2** Detailed photovoltaic parameters for DSSCs made with different photoanodes<sup>a</sup>

				$Z_{ m dif}$			
Cells	$R_1(\Omega)$	$R_{\mathrm{ct}}(\Omega)$	$C_1(F)$	$Y_{o}(S)$	$B(s^{1/2})$	$R_2(\Omega)$	$C_2(F)$
CLs CMs CSs CTs	35.53 42.33 46.81 48.60	1.47 2.30 2.91 82.5	5.24E-5 4.68E-5	6.46E-3 1.59E-2 1.10E-2 2.40E-3	1.84 1.61	47.23 36.32 42.76 48.69	6.1E-10 8.3E-10 1.3E-10 1.1E-11

<sup>a</sup>  $J_{sc}$ : short-circuit photocurrent.  $V_{sc}$ : open-circuit photovoltage. FF: fill factor.  $\eta$ : power conversion efficiency.

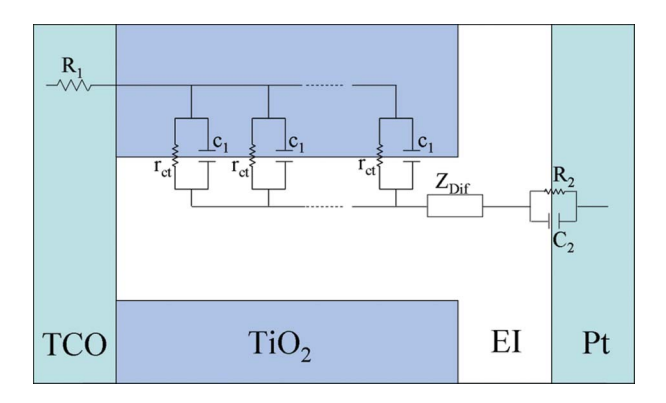


Fig. 7 The equivalent model used to represent the interfaces in 1-D DSSCs composed of TCO | sandwich-type photoelectrode-dye | I<sub>3</sub>-/I || Pt | TCO.

the interfacial resistance of the dye-sensitized photoelectrode  $I_3^-/I^-$  electrolyte interface, is 1.47  $\Omega$  for CLs, 2.30  $\Omega$  for CMS and 2.91  $\Omega$  for CSs. The lower interface resistance will result in faster interfacial electron transfer, which favours the higher  $\eta$ . The interface resistances of all sandwich-type structure solar cells are lower than that of CTs, so all these cells have higher interfacial electron transfer than CTs. Eventually, higher  $\eta$  of these sandwichtype structure solar cells are achieved. Amongst them, the CLs display the fastest electron transfer rate and thus the highest  $\eta$ . These results are in accordance with the photoelectrical conversion efficiency data discussed above.

## 2.5. Electron collection efficiency studied by the photovoltage transient

The photovoltage transient measurements offer a direct result about the electron collection efficiency and the interfacial charge recombination.<sup>38</sup> An electron/hole pair is generated after the laser illuminated the sample. The photo-generated electrons traverse to the TCO while the hole goes into the TiO<sub>2</sub> surface. The photovoltage is obtained when the electron/hole pair separates. The longer the distance that photo-generated electrons traverse, the stronger the photovoltage is. The whole photovoltage transient consists of the forward edge and decay process. From the forward edge, we can obtain the separation rate of the electron/hole pair and the time when the separation distance reaches a maximum, which scales the electron collection efficiency quantificationally. The decay process reflects the recombination rate of the electron/hole pair.

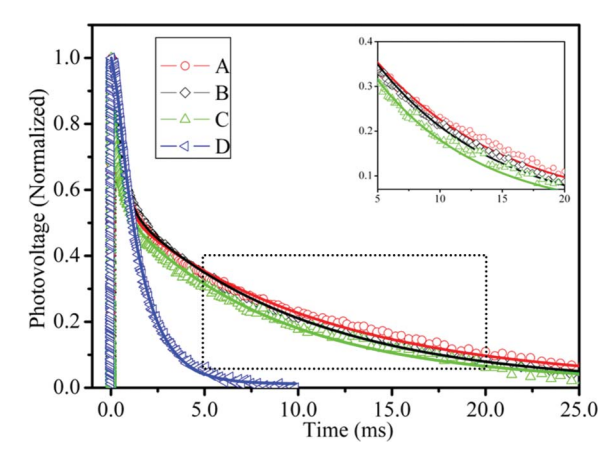


Fig. 8 The Photovoltage transient of dye-sensitized PLs (a), PMs (b), PSs (c) and PTs (d). Inset is the magnification of the partial photovoltage decay process curve.

Fig. 8 compares the photovoltage transient of the dye-sensitized sandwich-type photoelectrodes with different NB lengths. All of the curves were normalized because the absolute photovoltage transient values were not crucial for the rise time and the interfacial charge recombination. The rise time is 4.4 ms for the sensitized-PLs and is 3.7, 1.2 and 2.1 ms for sensitized-PMs, PSs and PTs, respectively. An increase in the uprising time indicates that the PLs have a better electron collection efficiency, i.e. the photo-generated electrons from the excited dye move a longer distance in PLs. Because the sensitized-PLs provide the longest electron transfer path, the photo-generated electrons move the longest distance compared to those in sensitized-PMs, PSs and PTs.

The photovoltage decay process is the electron/hole pair recombination process. When the electrons are injected into the conduction band of TiO<sub>2</sub>-B from the excited dye, they will recombine either with the dye cations or the surface traps of the  $TiO_2$ -B NBs. The number (N) of recombined electrons in unit time is in direct proportion to the number of electrons in the conduction band of TiO<sub>2</sub>-B:

$$\frac{dN}{dt} = -AN\tag{2}$$

where A is the Einstein decay coefficient. After integration, we get:

$$N = N_0 e^{-At} \tag{3}$$

where  $N_{\scriptscriptstyle 0}$  is the photo-generated electron number before decay. When  $\tau_s = \frac{1}{A}$ , which is defined as decay lifetime, so:

$$N = N_0 e^{-t/\tau_S},\tag{4}$$

When  $t = \tau_s$ :

$$N = \frac{N_0}{e} \tag{5}$$

It could be seen that the decay of all of photovoltage transients could be fitted well. The calculated lifetime is 10.7 ms for sensitized-PLs and 9.6, 8.5 and 1.4 ms for the sensitized-PMs, PSs and PTs, respectively. This indicates that the PLs could decrease the interfacial charge recombination compared to the PMs, PSs and PTs.

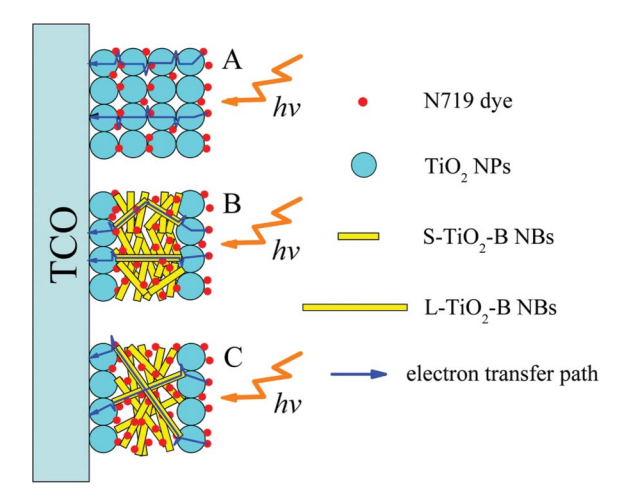


Fig. 9 schematic diagrams of the electron transfer path in the dye-sensitized TiO<sub>2</sub> NP photoelectrode (a), PSs (b) and PLs (c), respectively.

Fig. 9 shows schematic diagrams of the electron transfer path in the dye-sensitized TiO<sub>2</sub> NP photoelectrode (a), PSs (b) and PLs (c). For the TiO<sub>2</sub> NP photoelectrode, the photoelectrons were trapped by the particle boundary during the transport path. This would limit the transfer rate (Fig. 9 A). For the dye-sensitized PSs and PLs, the photoelectrons tended to undertake a convenient transfer path (Fig. 9b,c). Namely, the electrons transfer through the TiO<sub>2</sub>-B NBs, which reduces the probability that the photoelectrons are trapped by the nanoparticle boundary. The dye-sensitized PLs possessed the longest TiO<sub>2</sub>-B NBs among all of DSSCs, leading to the least electron transfer loss for PLs and the highest photoelectrical conversion efficiency for CLs.

#### **Conclusions** 3.

The conversion efficiency of dye-sensitized solar cells was improved effectively by using sandwich-type structure photoelectrodes, which consisted of one-dimensional TiO2-B NBs as a rapid electron transport layer and TiO<sub>2</sub> nanoparticles as a dye adsorption layer. The length of the TiO2-B in the sandwichstucture photoelectrode was demonstrated to critically influence the conversion efficiency of the DSSCs. The cells based on the longest TiO<sub>2</sub>-B NB/TiO<sub>2</sub> NP sandwich-type structure photoelectrodes (CLs) achieved the highest  $\eta$  of 7.94%, which was higher than that of the middle-length CMs (7.63%) and the short CSs (7.47%). Such an improved conversion efficiency of the longest TiO<sub>2</sub>-B NB sandwich-type DSSCs was ascribed to the best electron collection efficiency (4.4 ms), longest decay lifetime (10.7 ms) and the fastest interfacial electron transfer ( $R_{ct} = 1.47 \Omega$ ), as evidenced by the measurement of the photovoltage transient and EIS.

## Experimental

## 4.1. Chemicals

The commercial TiO<sub>2</sub> powder (Degussa P25) was purchased from standard sources and used as received. The Ru complex dye used was cis-bis(isothiocyanato)-bis (2,2'-bipyridyl-4,4'dicarboxylato)-ruthenium(II) bistetrabutylammonium (N719, Solaronix SA). The redox shuttle electrolyte was composed of 0.1 M LiI (anhydrous, 99%, Acros), 0.05 M I<sub>2</sub> (≥99.8%,

A. R.), 0.5 M *tert*-butylpyridine (99%, Aldrich) and 0.6 M 1-propyl-2,3-dimethylimidazolium iodide (99%, A. R.) in 3-methoxypropionitrile (99%, Fluka). The transparent conducting glass (TCO, F-doped  $SnO_2$  layer, sheet resistance =  $20~\Omega/\text{square}$ ) was used as received for the electrode substrate. The water used was ultrapure (18 M  $\Omega\cdot\text{cm}^{-2}$ ).

## 4.2. Synthesis of 1D TiO<sub>2</sub>-B NBs with different lengths

The long (10 µm) TiO<sub>2</sub>-B NBs (L-TiO<sub>2</sub>-B NBs) were synthesized *via* a facile hydrothermal method.<sup>39</sup> 7.2 g of TiO<sub>2</sub> (Degussa P25) were firstly dispersed in 40 mL of 15 M NaOH aqueous solution. After the solution was stirred for 1 h, the resulting suspension was transferred into a Teflon-lined stainless steel autoclave. The autoclave was maintained at 170 °C for 72 h and then cooled to room temperature naturally. The resulting white precipitate was recovered by centrifugation and washed with 0.1 M HCl solution and deionized water several times until pH = 7. Then they were dried at 80 °C. At last, they were calcinated at 450 °C for 30 min (ramping rate 1 °C min<sup>-1</sup>).

The synthesis of middle (4  $\mu$ m) TiO<sub>2</sub>-B NBs (M-TiO<sub>2</sub>-B NBs) used a solvothermal method. Firstly, 1 g of TiO<sub>2</sub> was dispersed in 60 mL of mixed solvents of 10 M NaOH aqueous solution and ethanol (volume ratio = 1:1). After the solution was stirred for 1 h, the resulting suspension was transferred into a Teflon-lined stainless steel autoclave. The autoclave was maintained at 180 °C for 16 h and then cooled to room temperature naturally. The following treatment of the resulting white precipitate was similar to that of the L-TiO<sub>2</sub>-B NBs. The synthesis of the short (500 nm) TiO<sub>2</sub>-B NBs (S-TiO<sub>2</sub>-B NBs) was similar to that of M-TiO<sub>2</sub>-B NBs, just adjusting the ethanol to diethanolamine.

## 4.3. Fabrication of photoelectrodes and the assembly of DSSCs

Four pastes were prepared, by homogeneously mixing the three kinds of TiO<sub>2</sub>-B NBs with different lengths and the TiO<sub>2</sub> NP (P25) into 2 mL of a TiO<sub>2</sub> colloid, respectively. The TiO<sub>2</sub> colloid was prepared following the previously published synthesis procedure. 40 A doctor-blade technique was used to fabricate the photoelectrodes. The sandwich structure photoanodes (PLs, PMs, PSs) consist of three-layer thin films, whose top and bottom layers were TiO<sub>2</sub> NP and the middle layer was TiO<sub>2</sub>-B NBs with different lengths (L-, Mand S-TiO<sub>2</sub>-B NBs). Moreover, as a reference, an electrode (PTs) with two-layers of TiO2 NP thin films was also prepared. After the first layer of film was sheared across a TCO substrate, they were calcinated at 450 °C for 30 min (ramping rate 1 °C min<sup>-1</sup>). Repetitive coating was carried out as the first electrodes cooled down to room temperature by repeating the above procedure. The sandwich-type structure photoelectrode is shown in Fig. 10. The thicknesses of all electrodes were determined to be around 15 µm. This is an appropriate thickness for the photoelectrode to get better power conversion efficiency, as indicated in the literature. 41,42 The sensitization of the photoelectrodes was achieved by immersing them into 0.5 mM N719 dye solution for 24 h.

The counter electrode was prepared following the previous work.<sup>43</sup> The dye-sensitized PLs, PMs, PSs and PTs and a Pt counter electrode were adhered together with epoxy resin, respectively. The space between the electrodes was filled with the electrolyte by capillary action.

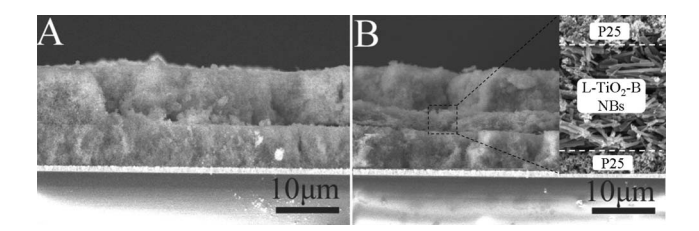


Fig. 10 SEM images of the electrode with two layers of  $TiO_2$  NPs (a) and the sandwich-type structure photoelectrodes (b). Inset in (b) is an enlarged sandwich-type structure.

## 4.4. Characterization

X-ray powder diffraction (XRD) patterns were obtained with a Bruker D8 diffractometer using Cu-K $\alpha$  ( $\lambda$  = 1.5406 Å) radiation. The accelerating voltage and the applied current were 40 kV and 20 mA, respectively. Raman spectra were recorded with a HR 800 micro-Raman spectrometer (Jobin Yvon, France) excited by an argon ion laser with a wavelength of 457.9 nm. Scanning electron microscopy (SEM) images were taken using a Hitachi S-4800 instrument operating at 15 kV. The transmission electron microscopy (TEM) experiment was performed on a JEM-3010 electron microscope (JEOL, Japan) with an acceleration voltage of 300 kV. Carbon-coated copper grids were used as the sample holders.

The Nitrogen adsorption/desorption isotherms were measured by TriStar II 3020 at 77 K. The specific surface area of L-TiO<sub>2</sub>-B NBs is 28.7 m<sup>2</sup> g<sup>-1</sup> and that of TiO<sub>2</sub> NPs (P25) is 49.1 m<sup>2</sup>/g. The surface photovoltage spectra (SPS) were carried out on a laboratory-built surface photovoltage spectroscopy. A 150 W xenon lamp with a monochromator was used as light source. The illumination direction was from the TiO<sub>2</sub> electrode. The generation of photovoltage arose from the creation of electron hole pairs followed by the separation under a built-in electric field (the space-charge layer).

The dye-sensitized photoelectrodes were desorbed in a 0.02 M NaOH solution in alcohol (EtOH) and H<sub>2</sub>O (volume ratio, 1:1) for 6 h to measure the adsorption dye amount. Photocurrent-photovoltage curves were recorded by a BAS100B electrochemical analyzer (Bioanalytical Systems Inc., USA). A 400 W xenon lamp with a UV filter was used as the light source. Its illumination intensity was about 40 mW cm<sup>-2</sup>. The irradiation area of DSSCs was about 0.12 cm<sup>2</sup>.

The EIS were performed with a computer-controlled IM6e impedance measurement unit (Zahner Elektrik, Germany). EIS were obtained by applying sinusoidal perturbations of 10 mV over the  $V_{\rm oc}$  at the frequency range from 0.05 to 100 KHz. All EIS measurements were carried out under illumination of 10 mW cm<sup>-2</sup>. The obtained spectra were fitted with ZsimpWin software in terms of appropriate equivalent circuits.

The photovoltage transient measurement was recorded on a TDS 5054 Digital Phosphor Oscilloscope (Tektronix, USA). A Polaris II Nd:YAG laser (New Wave Research Inc., USA) was used to excite the dye-sensitized PLs, PMs, PSs and PTs, respectively. The 532 nm wavelength of the laser was selected because the N719 dye has a maximal absorption at about 512 nm and the average energy of each laser pulse was about 100  $\mu$ J with a standard deviation of 20  $\mu$ J. The setup scheme and the principle of SPS

and the photovoltage transient were also shown in our previous work.40

## Acknowledgements

We gratefully acknowledge the support of this research by the Key Program Projects of the National Natural Science Foundation of China (21031001), the National Natural Science Foundation of China (20971040, 21001042, 20703015), the Cultivation Fund of the Key Scientific and Technical Innovation Project, Ministry of Education of China (708029), Program for New Century Excellent Talents in Heilongjiang Provincial University of China (1154-NCET-010), Harbin Youth Foundation (2009RFQXG202) and the Scientific Research Fund of Heilongjiang Provincial Education Department (11541283).

## References

- 1 B. O'Regan and M. Grätzel, Nature, 1991, 353, 737.
- 2 R. A. Kerr, Science, 2007, 318, 1230.
- 3 A Hagfeldt and M. Grätzel, Chem. Rev., 1995, 95, 49.
- 4 U Bach, D. Lupo, P. Comte, J. E. Moser, F. Weissortel, J. Salbeck, H. Spreitzer and M. Grätzel, Nature, 1998, 395, 583.
- 5 S Standridge, G. Schatz and J. Hupp, J. Am. Chem. Soc., 2009, 131, 8407.
- 6 M. K. Nazeeruddin, A. Kay, I. Rodicicio, R. Humphry-Baker, E. Muller, P. Liska, N. Vlachopoulos and M. Grätzel, J. Am. Chem. Soc., 1993, 115, 6382
- 7 J. R. Durrant, S. A. Haque and E. Palomares,, Coord. Chem. Rev., 2004, 248, 1247.
- 8 M. Grätzel, J. Photochem. Photobiol., C, 2003, 4, 145.
- 9 S. Y. Huang, G. Schlichthörl, A. J. Nozik, M. Grätzel and A. J. Frank, J. Phys. Chem. B, 1997, 101, 2576.
- 10 H. Qin, S. Wenger, M. Xu, F. Gao, X. Jing, P. Wang, S. M. Zakeeruddin and M. Grätzel, J. Am. Chem. Soc., 2008, 130, 9202.
- 11 S. Sodergren, A. Hagfeldt, J. Olsson and S. E. Lindquist, J. Phys. Chem., 1994, 98, 5552
- 12 L. M. Peter, J. Phys. Chem. C, 2007, 111, 6601.
- 13 B. C. O'Regan, K. Bakker, J. Kroeze, H. Smit, P. Sommeling and J. R. Durrant, J. Phys. Chem. B, 2006, 110, 17155.
- 14 A. Martinson, M. Goes, F. Fabregat-Santiago, J. Bisquert, M. Pellin and J. Hupp, J. Phys. Chem. A, 2009, 113, 4015.
- 15 M. Wei, Y. Konishi, H. Zhou, M. Yanagida, H. Sugihara and H. Arakawa, J. Mater. Chem., 2006, 16, 1287.
- 16 D. Chen, F. Huang, Y. B. Cheng and R. Caruso, Adv. Mater., 2009, 21, 2206.

- 17 Y. Zhang, Z. Xie and J. Wang, ACS Appl. Mater. Interfaces, 2009, 1,
- 18 J. Oh, J. Lee, H. Kim, S. Han and K. Park, Chem. Mater., 2010, 22, 1114.
- 19 B. Liu and E. S. Aydil, J. Am. Chem. Soc., 2009, 131, 3985.
- 20 C. Xu, X. Wang and Z. L. Wang, J. Am. Chem. Soc., 2009, 131,
- 21 C. Xu, P. Shin, L. Cao and D. Gao, J. Phys. Chem. C, 2010, 114, 125.
- 22 M. Law, L. E. Greene, J. C. Johnson, R. Saykally and P. Yang, Nat. Mater., 2005, 4, 455.
- 23 X. Feng, K. Shankar, O. K. Varghese, M. Paulose, T. J. Latempa and C. A. Grimes, Nano Lett., 2008, 8, 3781.
- 24 J. B. Baxter and E. S. Aydil, Sol. Energy Mater. Sol. Cells, 2006, 90,
- 25 B. Tan and Y. Wu, J. Phys. Chem. B, 2006, 110, 15932.
- 26 S. Pang, T. Xie, Y. Zhang, X. Wei, M. Yang, D. Wang and Z. Du, J. Phys. Chem. C, 2007, 111, 18417.
- 27 Q. Wang, Z. H. Wen and J. H. Li, Adv. Funct. Mater., 2006, 16,
- 28 K. Pan, Y. Dong, C. Tian, W. Zhou, G. Tian, B. Zhao and H. Fu, Electrochim. Acta, 2009, 54, 7350.
- 29 Y. V. Kolen'ko, K. A. kovnir, A. I. Gavrilov, A. V. Garshev, J. Frantti, O. I. Lebedev, B. R. Churagulov, G. V. Tendeloo and M. Yoshimura, J. Phys. Chem. B, 2006, 110, 4030.
- 30 T. P. Feist and P. K. Davies, J. Solid State Chem., 1992, 101, 275.
- 31 A. R. Armstrong, G. Armstrong, J. Canales and P. G. Bruce, Angew. Chem., Int. Ed., 2004, 43, 2286.
- 32 Y. Lin, D. Wang, Q. Zhao, M. Yang and Q. Zhang, J. Phys. Chem. C, 2004, 108, 3202.
- 33 M. Yanagida, T. Yamaguchi, M. Kurashige, K. Hara, R. Katoh, H. Sugihara and H. Arakawa, Inorg. Chem., 2003, 42, 7921.
- 34 F. Fabregat-Santiago, J. Bisquert, E. Palomares, L. Otero, D. Kuang, S. M. Zakeeruddin and M. Gratzel, J. Phys. Chem. C, 2007, 111, 6550.
- 35 C. Longo, A. F. Nogueira, M. A. De Paoli and H. Cachet, J. Phys. Chem. B, 2002, 106, 5925.
- Y. Qu, W. Zhou, K. Pan, C. Tian, Z. Ren, Y. Zhen and H. Fu, Phys. Chem. Chem. Phys., 2010, 12, 9205.
- 37 J. Qu, X. P. Gao, G. R. Li, Q. W. Jiang and T. Y. Yan, J. Phys. Chem. C, 2009, 113, 3359.
- 38 X. Wei, T. Xie, D. Xu, Q. Zhao, S. Pang and D. Wang, Nanotechnology, 2008, 19, 275707.
- 39 G. Armstrong, A. R. Armstrong, J. Canales and P. G. Bruce, Chem. Commun., 2005, 2454.
- 40 Z. Liu, K. Pan, Q. Zhang, R. Jia, Q. LV, D. Wang, Y. Bai and T. Li, Thin Solid Films, 2004, 468, 291.
- 41 P. Wang, S. M. Zakeeruddin, P. Comte, I. Exnar and M. Grätzel, J. Am. Chem. Soc., 2003, 125, 1166.
- 42 P. Wang, Q. Dai, S. M. Zakeeruddin, M. Forsyth, D. R. MacFarlane and M. Grätzel, J. Am. Chem. Soc., 2004, 126, 13590.
- 43 A. Hagfeldt and M. Grätzel, Acc. Chem. Res., 2000, 33, 269.